Dynamic Bifurcation in Dc Drives

K.T. Chau, J.H. Chen, C.C. Chan
Department of Electrical & Electronic Engineering,
The University of Hong Kong, Pokfulam Road, Hong Kong

Abstract — Dynamic bifurcation as well as chaotic behavior in a fixed-frequency current-mode controlled dc chopper-fed dc motor drive system is presented. The key is to derive an iterative map that describes the nonlinear dynamics of the system operating in the continuous conduction mode. It illustrates that different bifurcation diagrams can be obtained by varying different system parameters. Analytical modeling of period-1 and hence period-*p* orbits as well as their stability analysis using the characteristic multipliers are also presented. Hence, those stable ranges of various system parameters can be determined. Moreover, chaotic behavior is quantified by evaluating the Lyapunov exponents. The proposed approach is so general that it can readily be applied to other current-mode dc drives.

I. INTRODUCTION

It has been well known that many current-mode controlled dc-dc converters are prone to instability [1], [2]. Until recently, it has been shown that what has been referred as instability is in fact chaos [3]-[5].

Since linear system theory is ill-suited to investigate the subharmonics and chaotic phenomena occurred in power electronics circuits, the most attractive approach has been the iterative nonlinear mapping. The one-dimensional mapping was successfully employed to derive the chaotic region of switching dc-dc converters in which the load was assumed as constant-voltage sink [3]-[5]. However, this load voltage is usually non-constant for practical switching dc-dc converters, leading to be a second-order rather than a first-order system.

Recently, the two-dimensional mapping has been manipulated to investigate the chaotic behavior of current-mode controlled boost converter [6], [7]. However, these studies have been limited to the use of constant current reference. Notice that this current reference is practically variable, depending on the output voltage deviation.

On the other hand, the investigation onto chaotic behavior of industrial motor drives has been surprisingly little. Nevertheless, the chaotic behavior of PWM inverter-fed induction motor drives has recently been investigated by using numerical analysis [8]. It has also been attempted to investigate the chaotic behavior of brushless dc motor drives by ignoring the switching effect and approximately transforming into the Lorenz system [9]. To the best of the authors' knowledge, analytical investigation onto industrial motor drives is absent in power electronics literature. The major reason should be due to the complexity of analytical formulation when considering the nonlinearity caused by the switching effect.

It is the purpose of this paper to investigate, both numerically and analytically, the nonlinear dynamics and chaotic behavior of industrial motor drives without ignoring the switching effect or accepting rough assumptions. A current-mode buck-type dc chopper-fed permanent-magnet (PM) dc motor drive is targeted for investigation which forms the basis for investigating other industrial motor drives.

Firstly, a two-dimensional iterative map that describes the nonlinear dynamics of a second-order dc drive system operating in the continuous condition mode will be derived. This derivation will cover all possible solutions, such as real and complex roots, to handle different system parameters and conditions. The presentation not only embraces the dynamic bifurcation of the rotational speed and armature current of the motor but also the duty cycle of the dc chopper. Secondly, analytical modeling of the period-1 and hence the generalized period-*p* orbits as well as their stability analysis will be presented. Thirdly, based on the derived iterative map, computer simulations will be carried out to study the dynamic bifurcation and chaotic behavior. Finally, theoretical results will be verified by PSpice simulation.

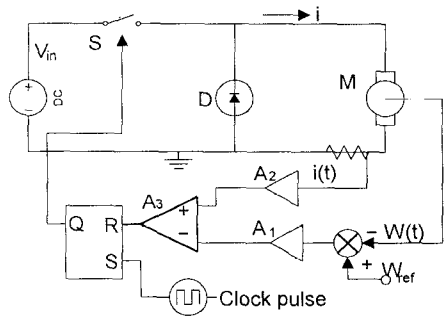

Fig. 1. Schematic diagram of dc drive.

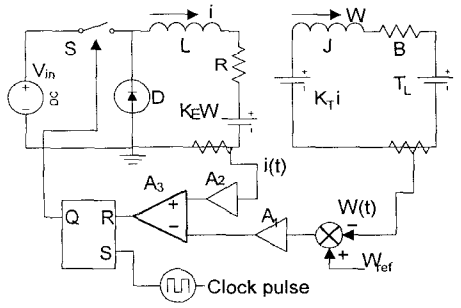

Fig. 2. Equivalent circuit of dc drive.

0-7803-3840-5/97/$10.00 © 1997 IEEE

II. Modeling of Drive Systems

As shown in Fig. 1, a fixed-frequency current-mode controlled buck-type dc chopper-fed PM dc motor drive operating in the continuous condition mode is used for exemplification. The corresponding equivalent circuit is shown in Fig. 2 which will be used throughout the analysis.

Consider that the operational amplifier A_1 and A_2 have gains g_ω and g_i, the speed and current control signals v_ω and v_i can be expressed as

$$v_\omega(t) = g_\omega(\omega_{ref} - \omega(t)) \tag{1}$$

$$v_i(t) = g_i i(t) \tag{2}$$

where $i(t)$, $\omega(t)$ and ω_{ref} are armature current, speed and reference speed of the dc motor, respectively. Then, both v_ω and v_i are fed into the comparator A_3 which outputs the pulse to the reset of an R-S latch. The power switch S is controlled by this R-S latch which is set by clock pulses of period T. Once the latch is set by the clock pulse, S is turned on and diode D is off. Then, S will keep closed until v_i exceeds v_ω where the latch begins to reset. When the latch is reset, S is turned off and D is on. Then, S remains open until the arrival of the next clock pulse where it will be closed again. If both set and reset signals occur simultaneously, the reset will dominate the set so that S keeps open until the occurrence of another clock pulse. Therefore, the system equation can be divided into two stages as given by

- Stage 1 (setting the latch):

$$\frac{d}{dt}\begin{pmatrix}\omega(t)\\ i(t)\end{pmatrix} = \begin{pmatrix}-B/J & K_T/J\\ -K_E/L & -R/L\end{pmatrix}\begin{pmatrix}\omega(t)\\ i(t)\end{pmatrix} + \begin{pmatrix}-T_l/J\\ V_{in}/L\end{pmatrix} \tag{3}$$

- Stage 2 (resetting the latch at $v_i > v_\omega$):

$$\frac{d}{dt}\begin{pmatrix}\omega(t)\\ i(t)\end{pmatrix} = \begin{pmatrix}-B/J & K_T/J\\ -K_E/L & -R/L\end{pmatrix}\begin{pmatrix}\omega(t)\\ i(t)\end{pmatrix} + \begin{pmatrix}-T_l/J\\ 0\end{pmatrix} \tag{4}$$

where R is armature resistance, L armature inductance, V_{in} dc supply voltage, K_E back-EMF constant, K_T torque constant, B viscous damping, J load inertia, and T_l load torque.

By defining the state vector $\mathbf{X}(t)$ and the following matrices $\mathbf{A}$, $\mathbf{E}_1$, $\mathbf{E}_2$ as

$$\mathbf{A} = \begin{pmatrix}-B/J & K_T/J\\ -K_E/L & -R/L\end{pmatrix},\quad \mathbf{X}(t) = \begin{pmatrix}\omega(t)\\ i(t)\end{pmatrix} \tag{5}$$

$$\mathbf{E}_1 = \begin{pmatrix}-T_l/J\\ V_{in}/L\end{pmatrix},\quad \mathbf{E}_2 = \begin{pmatrix}-T_l/J\\ 0\end{pmatrix} \tag{6}$$

the system equation given by (3) and (4) can then be rewritten as

$$\dot{\mathbf{X}}(t) = \mathbf{A}\,\mathbf{X}(t) + \mathbf{E}_k \qquad (k = 1,2) \tag{7}$$

Since k is topological dependent, hence time dependent, the system equation given by (7) is in fact a time-varying state equation. Thus, this closed-loop drive system is a second-order non-autonomous dynamical system.

III. Derivation of Poincaré Map

Given the desired initial conditions $\mathbf{X}(t_0)$, the analytical solution of the system equation given by (7) can be expressed as

$$\begin{aligned}\mathbf{X}(t) &= \Phi(t-t_0)\mathbf{X}(t_0) + \int_{t_0}^{t}\Phi(t-\tau)\mathbf{E}_k d\tau \\ &= -\mathbf{A}^{-1}\mathbf{E}_k + \Phi(t-t_0)(\mathbf{X}(t_0) + \mathbf{A}^{-1}\mathbf{E}_k) \quad (k = 1,2)\end{aligned} \tag{8}$$

where $\Phi(t) = e^{\mathbf{A}t}$ is so-called the state transition matrix.

By defining the following parameters

$$\alpha = \frac{1}{2}\left(\frac{R}{L} + \frac{B}{J}\right),\quad \Delta = \frac{1}{4}\left(\frac{R}{L} - \frac{B}{J}\right)^2 - \frac{K_E K_T}{LJ} \tag{9}$$

the eigenvalues λ_1, λ_2 of the matrix $\mathbf{A}$ can be expressed as

for $\Delta = 0$, $\lambda_1 = \lambda_2 = \lambda = -\alpha$ (10)

for $\Delta > 0$, $\lambda_1 = -\alpha + \sqrt{\Delta}$, $\lambda_2 = -\alpha - \sqrt{\Delta}$ (11)

for $\Delta < 0$, $\lambda_1 = -\alpha + j\sqrt{-\Delta}$, $\lambda_2 = -\alpha - j\sqrt{-\Delta}$ (12)

Hence, the corresponding state transition matrix can be obtained as

for $\Delta = 0$, $\Phi(t) = e^{-\alpha t}[\mathbf{1} - t(2\alpha\mathbf{1} - \mathbf{A})]$ (13)

for $\Delta > 0$, $\Phi(t) = \frac{1}{\lambda_2 - \lambda_1}[e^{\lambda_1 t}(\lambda_2\mathbf{1} - \mathbf{A}) - e^{\lambda_2 t}(\lambda_1\mathbf{1} - \mathbf{A})]$ (14)

for $\Delta < 0$, $\Phi(t) = e^{-\alpha t}[\mathbf{1}\cos(\beta t) + \frac{1}{\beta}(\alpha\mathbf{1} + \mathbf{A})\sin(\beta t)]$ (15)

where $\mathbf{1}$ is the identity matrix and $\beta = \sqrt{-\Delta}$.

As shown in Fig. 3, the interval of closing or opening switch may be longer than a clock cycle under certain conditions. Thus, $\mathbf{X}(t)$ is generally sampled at the beginning of the clock pulse that makes S changing from off to on, instead of every clock cycle. Hence, the drive system always operates in Stage 1 first and then in Stage 2 for each sampling interval. By denoting the corresponding discrete state vector as $\mathbf{X}_n$, the iterative function that maps this vector to its successive one $\mathbf{X}_{n+1}$ is called the Poincaré map which is defined as P: $\Re^2 \to \Re^2$

$$\mathbf{X}_{n+1} = P(\mathbf{X}_n) \tag{16}$$

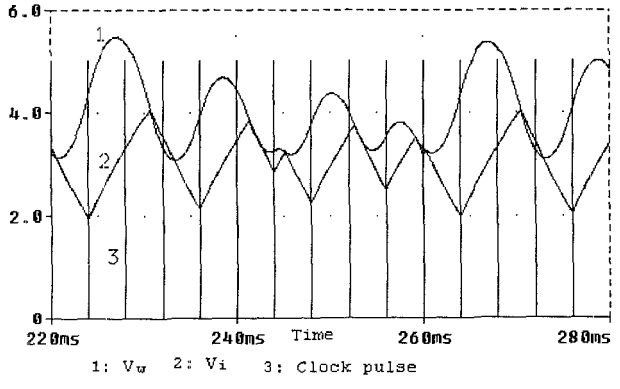

Fig. 3. Chaotic waveforms of v_ω and v_i against clock pulse.

By defining the intervals of Stages 1 and 2 as δT and $\delta' T$, respectively, the interval of Poincaré map becomes $mT=(\delta+\delta')T$. Thus, $\mathbf{X}(\delta T)$ and $\mathbf{X}_{n+1}$ can be directly derived from (8) as given by

$$\mathbf{X}(\delta T) = -\mathbf{A}^{-1}\mathbf{E}_1 + \Phi(\delta T)(\mathbf{X}_n + \mathbf{A}^{-1}\mathbf{E}_1) \tag{17}$$

$$\mathbf{X}_{n+1} = -\mathbf{A}^{-1}\mathbf{E}_2 + \Phi(mT - \delta T)(\mathbf{X}(\delta T) + \mathbf{A}^{-1}\mathbf{E}_2) \tag{18}$$

Using (1) and (2), δ can be determined by evaluating the solution of the following transcendental equation

$$\begin{aligned} h(\delta) &= g_i i(\delta T) - g_\omega(\omega_{ref} - \omega(\delta T)) \\ &= \mathbf{E}_3(\mathbf{X}(\delta T) - \mathbf{E}_4) = 0 \end{aligned} \tag{19}$$

where $\mathbf{E}_3=(g,\ 1)$, $g=g_\omega / g_i$, and $\mathbf{E}_4=(\omega_{ref},\ 0)$. On the other hand, m can be obtained as the minimum integer which is larger than δ and fulfills $h(m)<0$. Hence, the Poincaré map can be written as

$$\begin{aligned} \mathbf{X}_{n+1} &= -\mathbf{A}^{-1}\mathbf{E}_1 + \Phi(mT)(\mathbf{X}_n + \mathbf{A}^{-1}\mathbf{E}_1) \\ &\quad + (\mathbf{1} - \Phi(mT - \delta T))\mathbf{A}^{-1}(\mathbf{E}_1 - \mathbf{E}_2) \end{aligned} \tag{20}$$

It should be noted that the above Poincaré map is derived from the analytical solution of the model of dc drive systems which covers all possible solutions such as real and complex roots due to different system parameters and conditions. Thus, this Poincaré map can be considered as the map for any second-order dynamical systems using similar mathematical models, such as other dc motor drives. Moreover, the derivation can readily be extended to those higher-order dynamical systems involving power switches.

IV. Analysis of Dynamic Bifurcation

Based on the above Poincaré map, dynamic bifurcation of the drive system can readily be investigated by employing standard numerical techniques such as the brute-force algorithm [10]. The investigation is mainly based on the generation of bifurcation diagrams with respect to various system parameter variations. However, the corresponding numerical simulation may take lengthy computational time because every iterative computation of the Poincaré map needs to solve the transcendental equation.

In order to avoid the lengthy computation and to attain an insight into the chaotic behavior, the approach to obtaining analytical solution of the Poincaré map with m=1 is described as follows.

A. Analysis of periodic solution and its stability

The steady-state periodic solution of the dc drive system is a fixed point, so-called the period-1 orbit $\mathbf{X}^*$, as given by

$$\mathbf{X}^* = P(\mathbf{X}^*) \tag{21}$$

Substituting (20) into (21), the fixed point can be obtained as

$$\mathbf{X}^* = -\mathbf{A}^{-1}\mathbf{E}_1 + (\mathbf{1} - \Phi(T))^{-1}(\mathbf{1} - \Phi(T - \delta T))\mathbf{A}^{-1}(\mathbf{E}_1 - \mathbf{E}_2) \tag{22}$$

Also, substituting of (22) into (19), δ can be determined from the corresponding transcendental equation

$$\begin{aligned} h(\delta) = \mathbf{E}_3[&-\mathbf{A}^{-1}\mathbf{E}_1 + \Phi(\delta T)(\mathbf{1} - \Phi(T))^{-1} \\ &(\mathbf{1} - \Phi(T - \delta T))\mathbf{A}^{-1}(\mathbf{E}_1 - \mathbf{E}_2) - \mathbf{E}_4] = 0 \end{aligned} \tag{23}$$

Hence, provided that the solution $0<\delta<1$ of (23) exists, $\mathbf{X}^*$ can be obtained from (22). Its characteristic multipliers (λ_1, λ_2) are the eigenvalues of the Jacobian matrix of that mapping (20), which is given by

$$\begin{aligned} DP(\mathbf{X}^*) &= \Phi(T) - \frac{\partial \Phi(T - \delta T)}{\partial \delta}\mathbf{A}^{-1}(\mathbf{E}_1 - \mathbf{E}_2)\frac{\partial \delta}{\partial \mathbf{X}^*} \\ &= \Phi(T) + \Phi(T - \delta T)(\mathbf{E}_1 - \mathbf{E}_2)T\frac{\partial \delta}{\partial \mathbf{X}^*} \end{aligned} \tag{24}$$

where $\dfrac{\partial \delta}{\partial \mathbf{X}^*} = \left(\dfrac{\partial \delta}{\partial \omega}, \dfrac{\partial \delta}{\partial i}\right)$. According to the implicit-function theorems, $\dfrac{\partial \delta}{\partial \mathbf{X}^*}$ can be deduced from (19) as

$$\begin{aligned} \frac{\partial \delta}{\partial \mathbf{X}^*} &= -\left(\frac{\partial h}{\partial \delta}\right)^{-1}\frac{\partial h}{\partial \mathbf{X}^*} \\ &= -[\mathbf{E}_3\Phi(\delta T)(\mathbf{A}\mathbf{X}^* + \mathbf{E}_1)T]^{-1}\mathbf{E}_3\Phi(\delta T) \end{aligned} \tag{25}$$

It is known that the fixed point of the mapping is stable if and only if its characteristic multipliers all lie within the unit circle in the complex plane. If one of their magnitudes equals unity, this fixed point can be a bifurcation point.

When the switching frequency is much greater than the magnitude of eigenvalues of the matrix $\mathbf{A}$, the transition matrix $\Phi(\delta T)$ can be approximated as $\Phi(\delta T) = \mathbf{1} + \delta T\mathbf{A}$, and the duty cycle δ can then deduced from (23) as given by

$$\delta = \frac{\mathbf{E}_3(\mathbf{A}^{-1}\mathbf{E}_2 + \mathbf{E}_4)}{T\mathbf{E}_3(\mathbf{1} - \Phi(T))^{-1}(\mathbf{E}_1 - \mathbf{E}_2)} \tag{26}$$

Hence, δ can be evaluated explicitly rather than solving from the transcendental equation, and can greatly facilitate the determination of those stable ranges of various system parameters.

B. Analysis of subharmonic solution and its stability

The subharmonic solution of the dc drive system is a cycle point, so-called the period-p orbit $\{\mathbf{X}_1^*, \cdots, \mathbf{X}_p^*\}$ (p>1), as given by

$$\mathbf{X}_{k+1}^* = P(\mathbf{X}_k^*) \quad (k = 1, \cdots, p-1), \quad \mathbf{X}_1^* = P(\mathbf{X}_p^*) \tag{27}$$

By defining δ_k $(k = 1, \cdots, p)$ as the duty ratio in the kth interval of the mapping, the p-fold iterative Poincaré map can be obtained as

$$\begin{aligned} \mathbf{X}_{n+p} &= P^{(p)}(\mathbf{X}_n) \\ &= -\mathbf{A}^{-1}\mathbf{E}_1 + \Phi(pT)(\mathbf{X}_n + \mathbf{A}^{-1}\mathbf{E}_1) \\ &\quad + \sum_{j=1}^{p}[\Phi((p-j)T)(\mathbf{1} - \Phi(T - \delta_j T))]\mathbf{A}^{-1}(\mathbf{E}_1 - \mathbf{E}_2) \end{aligned} \tag{28}$$

By using (27), the period-p orbit can then be derived as

$$\mathbf{X}_1^* = -\mathbf{A}^{-1}\mathbf{E}_1 + (\mathbf{1}-\Phi(pT))^{-1}\sum_{j=1}^{p}[\Phi((p-j)T)(\mathbf{1}-\Phi(T-\delta_j T))]\mathbf{A}^{-1}(\mathbf{E}_1-\mathbf{E}_2) \quad (29)$$

$$\mathbf{X}_i^* = -\mathbf{A}^{-1}\mathbf{E}_1 + \Phi((i-1)T)(\mathbf{X}_1^* + \mathbf{A}^{-1}\mathbf{E}_1) + \sum_{j=1}^{i-1}[\Phi((i-j-1)T)(\mathbf{1}-\Phi(T-\delta_j T))\mathbf{A}^{-1}(\mathbf{E}_1-\mathbf{E}_2)] \quad (i=2,\cdots,p) \quad (30)$$

$$h_i(\mathbf{d}) = \mathbf{E}_3[-\mathbf{A}^{-1}\mathbf{E}_1 + \Phi(\delta_i T)(\mathbf{X}_i^* + \mathbf{A}^{-1}\mathbf{E}_1) - \mathbf{E}_4] = 0 \quad (i=1,\cdots,p) \quad (31)$$

where $\Phi(0)=\mathbf{1}$ and $\mathbf{d}=(\delta_1,\cdots,\delta_p)$. By substituting (29) and (30) into (31), $\mathbf{d}$ can be determined. Provided that the solution of $0<\delta_i<1$ (i=1,$\cdots$,p) exists, $\mathbf{X}_1^*,\cdots,\mathbf{X}_p^*$ can then be obtained from (29) and (30). Due to the cyclic property of a cycle point, $\{\mathbf{X}_2^*,\cdots,\mathbf{X}_p^*,\mathbf{X}_1^*\}$, $\cdots$, $\{\mathbf{X}_p^*,\mathbf{X}_1^*,\cdots,\mathbf{X}_{p-1}^*\}$ are also period-p orbits which correspond to the same subharmonic frequency. If $\mathbf{X}_1^*=\cdots=\mathbf{X}_p^*$, the period-$p$ orbit becomes the period-1 orbit, which shows that period-1 is its subset.

For the period-p orbits $\{\mathbf{X}_1^*,\cdots,\mathbf{X}_p^*\}$, $\mathbf{X}_1^*$ is a fixed point of the p-fold iterative Poincaré map. Therefore, its characteristic multipliers (λ_1, λ_2) are the eigenvalues of the Jacobian matrix of that mapping, which is given by

$$DP^{(p)}(\mathbf{X}_1^*) = \Phi(pT) + \sum_{j=1}^{p}[\Phi((p-j)T)\Phi(T-\delta_j T)(\mathbf{E}_1-\mathbf{E}_2)T\frac{\partial\delta_j}{\partial\mathbf{X}_1^*}] \quad (32)$$

By substituting (30) into (31), it results

$$\mathbf{H}(\mathbf{d},\mathbf{X}_1^*) = [h_1(\mathbf{d},\mathbf{X}_1^*),\cdots,h_p(\mathbf{d},\mathbf{X}_1^*)]^T = \mathbf{0} \quad (33)$$

Hence, according to the implicit-function theorems, the partial derivative in (32) can be expressed as

$$\frac{\partial\mathbf{d}}{\partial\mathbf{X}_1^*} = \left(\frac{\partial\delta_1}{\partial\mathbf{X}_1^*},\cdots,\frac{\partial\delta_p}{\partial\mathbf{X}_1^*}\right)^T = -\left[\frac{\partial\mathbf{H}}{\partial\mathbf{d}}\right]^{-1}\left[\frac{\partial\mathbf{H}}{\partial\mathbf{X}_1^*}\right] \quad (34)$$

where

$$\frac{\partial\mathbf{H}}{\partial\mathbf{d}} = \left[\frac{\partial h_i}{\partial\delta_j}\right]_{p\times p} = diag[\mathbf{E}_3\Phi(\delta_i T)(\mathbf{A}\mathbf{X}_i^*+\mathbf{E}_1)T] + [\mathbf{E}_3\Phi(\delta_i T)\Phi((i-j)T-\delta_j T)(\mathbf{E}_1-\mathbf{E}_2)T]_{p\times p} \quad (35)$$

$$\frac{\partial\mathbf{H}}{\partial\mathbf{X}_1^*} = \left[\frac{\partial h_1}{\partial\mathbf{X}_1^*},\cdots,\frac{\partial h_p}{\partial\mathbf{X}_1^*}\right]^T = [\mathbf{E}_3\Phi(\delta_1 T),\cdots,\mathbf{E}_3\Phi((p-1)T+\delta_p T)]^T \quad (36)$$

Notice that $\Phi((i-j)T-\delta_j T)$ in (35) becomes a zero matrix when $j\geq i$.

C. Lyapunov exponents

Lyapunov exponents are a generalization of the characteristic multipliers. They are used to determine the stability of any type of steady-state behavior including chaos. For a two-dimensional discrete-time mapping $P(\mathrm{X})$, the matrix $\mathbf{M}_n$ is defined as

$$\mathbf{M}_n = \prod_{i=0}^{n-1} DP(\mathbf{X}_i) \quad (37)$$

where $DP(\mathbf{X}_i)$ is Jacobian matrix of the mapping. Then, the Lyapunov exponents $\mathbf{L}=(\lambda_1,\ \lambda_2)$ are defined as

$$\mathbf{L} = \lim_{n\to\infty}\frac{1}{n}\log|\text{eigenvalues of } \mathbf{M}_n| \quad (38)$$

The mapping is of a strange attractor if and only if at least one of the Lyapunov exponents is positive.

According to the Poincaré map in (20) as well as its Jacobian matrix given by (24) and (25), the corresponding Lyapunov exponents can readily be evaluated from (37) and (38).

V. Computer Simulation

To illustrate the derived iterative maps, computer simulation of various bifurcation diagrams is carried out. The nominal system parameters are based on the following values: T=4ms, V_{in}=100V, g_i=1, g_ω=2, g=2, R=3.5Ω, L=66mH, K_E=0.1356V/rads^{-1}, K_T=0.1324Nm/A, B=0.000164Nm/rads^{-1}, J=0.000571Nm/rads^{-2}, T_l=0.39Nm, ω_{ref}=100rads^{-1}.

A. Bifurcation diagrams using numerical computation

By employing standard numerical techniques such as the brute-force algorithm to compute the Poincaré map given by (19) and(20), bifurcation diagrams of the speed ω and armature current i versus input voltage V_{in} and gain g can be resulted as shown in Figs. 4 to 7, respectively. The corresponding distribution of the duty ratios δ and δ' with respect to V_{in} and g are also shown in Figs. 8 to 11.

It can be found that the system exhibits a typical period-doubling route to chaos, covering both chaotic speed and current. As shown in Figs. 6 and 7, it is interesting to note that the period-2 orbit bifurcates to the period-3 because of the discontinuities of δ which must be positive as shown in Fig. 10. Moreover, as shown in Figs. 8 and 9, as V_{in} successively decreases, δ may be greater than unity during chaos while δ' is always less than unity. On the contrary, as shown in Figs. 10 and 11, as g gradually increases, δ is always less than 1 while δ' may be greater than unity during chaos. As shown in Fig. 3, when V_{in}=45V and g=3, both δ and δ' may be greater that unity. It indicates that the chaotic behavior exists when at least one of the duty ratios δ and δ' is greater than unity.

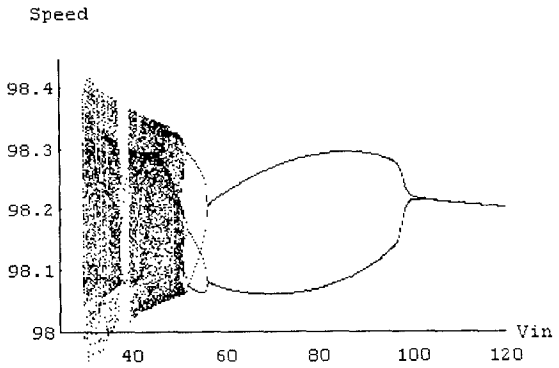

Fig. 4. Bifurcation diagram of speed versus input voltage.

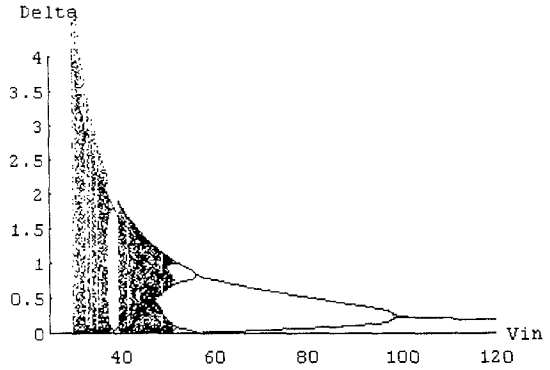

Fig. 8. Distribution of δ versus input voltage.

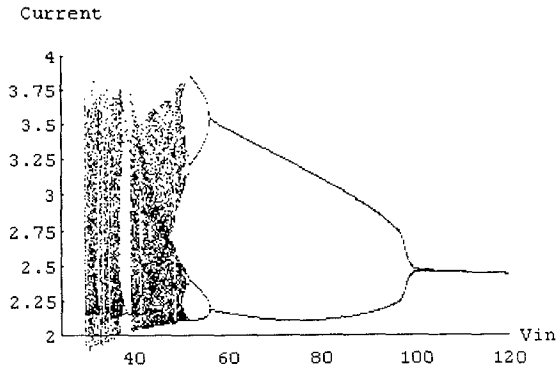

Fig. 5. Bifurcation diagram of current versus input voltage.

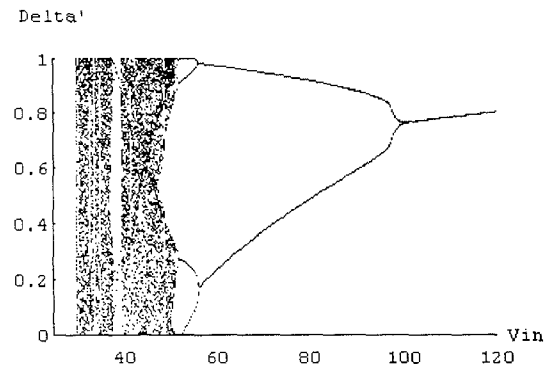

Fig. 9. Distribution of δ' versus input voltage.

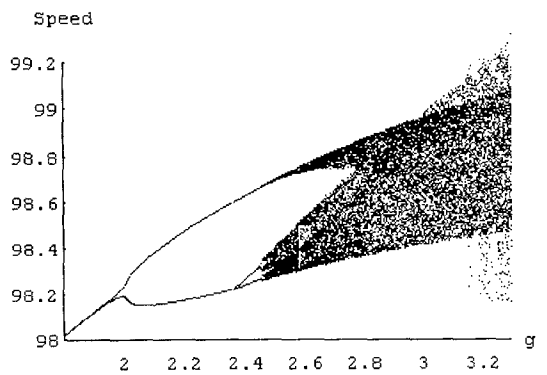

Fig. 6. Bifurcation diagram of speed versus gain.

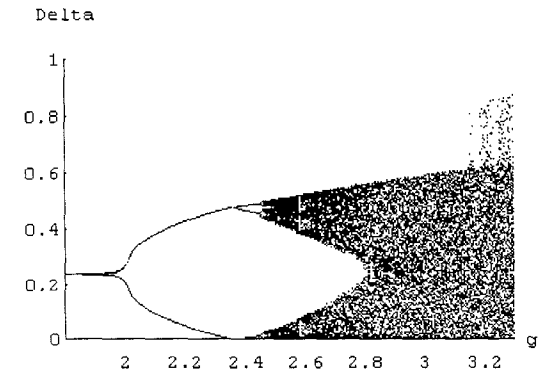

Fig. 10. Distribution of δ versus gain.

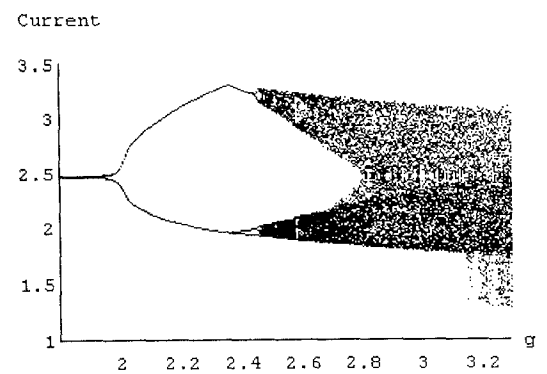

Fig. 7. Bifurcation diagram of current versus gain.

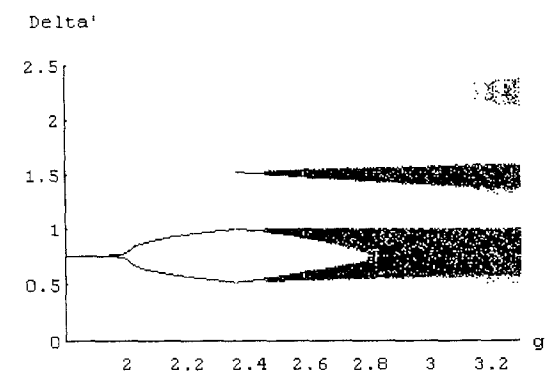

Fig. 11. Distribution of δ' versus gain.

The strange attractor of the armature current versus motor speed with V_{in}=45V is also displayed in Fig. 12. Its Lyapunov exponents are 0.655 and –2.73.

B. Bifurcation diagrams using analytical approach

Based on the derived period-1 orbit as given by (24)-(26), the duty ratio δ and the corresponding characteristic multipliers $|\lambda_1, \lambda_2|$ for V_{in} varying from 30V to 200V and g from 1 to 5 are shown in Figs. 13 and 14, respectively. It can be found that one of the magnitudes is greater than 1 when V_{in}<102V or g>2, indicating that the period-1 orbit is unstable when V_{in}<102V or g>2. The 3-D surface plot of the value λ of max$|\lambda_1, \lambda_2|$ with respect to V_{in} and g is shown in Fig. 15 in which all λ are digitized to be zero for those values less than unity or to be unity for those higher than unity. Hence, the stable region can be identified as the zone with zero height.

By substituting p=2 into (31), the solution of $\delta=\{\delta_1, \delta_2\}$ for a range of V_{in} from 50V to 120V is shown in Fig. 16. By using (32)-(36) with p=2, $|\lambda_1, \lambda_2|$ can be obtained as shown in Fig. 17. It can be found that the period-2 orbit is stable provided that V_{in} lies between 56.3V and 102V. Similarly, the corresponding stable range of g lies between 2 and 2.36.

It should be noted that the above analytical results closely agree with the previous numerical results. It is obvious that the required computational time based on the derived analytical solution is extremely less than that required for computation using the numerical brute-force algorithm. Thus, the proposed analytical approach can greatly facilitate the identification of the desired stable operating ranges for different system parameters and conditions.

C. PSpice verification

Based on the same operating parameters and conditions, realistic PSpice simulation of the drive system is performed. As shown in Fig. 18, the PSpice-simulated waveforms of v_ω, v_i and clock pulse at V_{in}=90V illustrate that the system is operating at the period-2 orbit with m=1. When V_{in}=45V, the phase plane trajectory of i versus ω is shown in Fig. 19, indicating that it is in chaos. These system behaviors closely agree with the previous theoretical bifurcation diagrams.

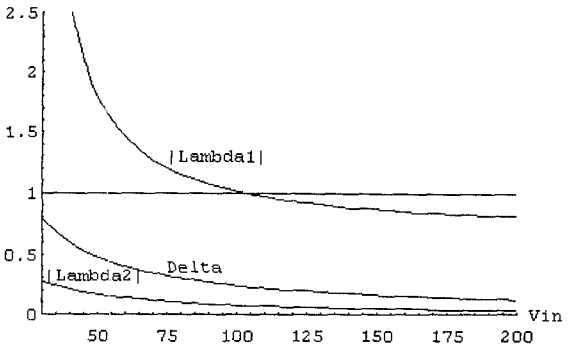

Fig. 13. δ and $|\lambda_1, \lambda_2|$ versus V_{in} for period-1 orbit.

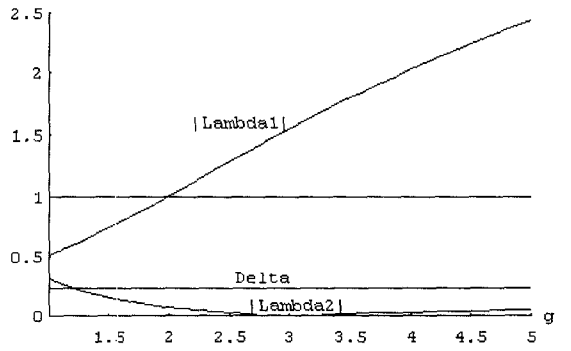

Fig. 14. δ and $|\lambda_1, \lambda_2|$ versus g for period-1 orbit.

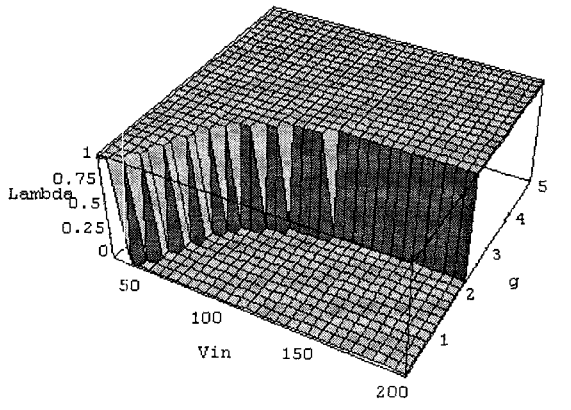

Fig. 15. Max$|\lambda_1, \lambda_2|$ versus V_{in} and g for period-1 orbit.

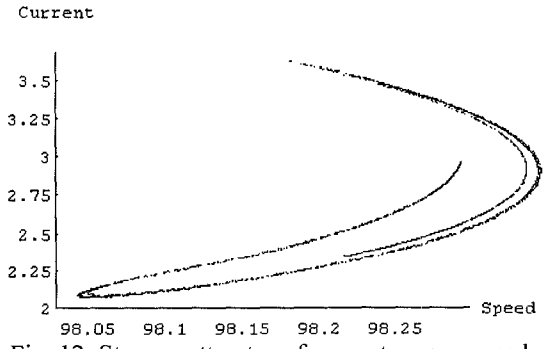

Fig. 12. Strange attractor of current versus speed.

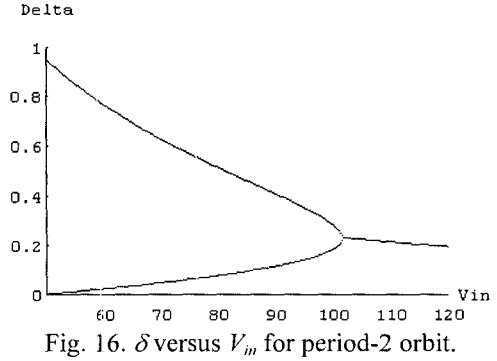

Fig. 16. δ versus V_{in} for period-2 orbit.

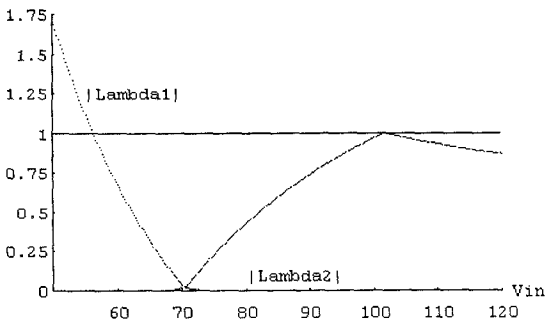

Fig. 17. $|\lambda_1, \lambda_2|$ versus V_{in} for period-2 orbit.

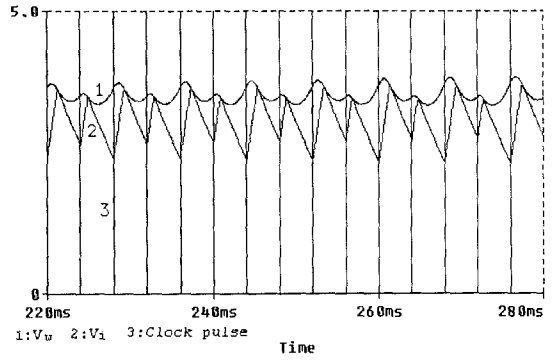

Fig. 18. PSpice v_ω , v_i and clock pulse for period-2 orbit.

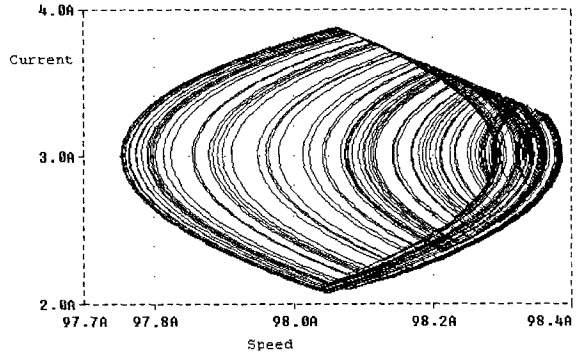

Fig. 19. PSpice trajectory of current versus speed in chaos.

VI. Conclusion

In this paper, a second-order iterative map that describes the nonlinear dynamics of the drive system operating in the continuous condition mode has been derived. Based on the derived map, computer simulation reveals that the system exhibits a typical period-doubling route to chaos. Also, the investigation onto the duty ratios δ and δ' during switch-on and switch-off provides a tool to identify whether the input voltage V_{in} or gain g causes the chaotic operation. Moreover, analytical modeling of the period-1 and period-p orbits as well as their stability analysis have been carried out. The key is on the analytical evaluation of characteristic multipliers. With the use of the proposed analytical approach, the identification of the desired stable operating ranges for different system parameters and conditions can be easily performed, without involving any lengthy numerical iteration. The theoretical results have also been verified by comparing with the bifurcation points occurred in PSpice simulation.

Although the investigation has been focused on a typical dc drive system, the proposed approach and derived equations can readily be applied or extended to other dc drive systems.

Acknowledgment

This work was supported and funded in part by the Committee on Research and Conference Grants, the University of Hong Kong.

References

[1] S. Hsu, A.R. Brown, L. Resnick and R.D. Middlebrook, "Modeling and analysis of switch dc-to-dc converters in constant-frequency current-programmed mode," *IEEE PESC Record*, 1979, pp. 284-301.

[2] R. Redl and I. Novak, "Instabilities in current-mode controlled switch voltage regulators," *IEEE PESC Record*, 1981, pp.17-28.

[3] J.H.B. Deane and D.C. Hamill, "Instability, subharmonics, and chaos in power electronic systems," *IEEE Transactions on Power Electronics*, vol. 5, 1990, pp. 260-268.

[4] J.H.B. Deane and D.C. Hamill, "Chaotic behavior in current-mode controlled dc-dc converter," *Electronics Letters*, vol. 27, 1991, pp. 1172-1173.

[5] D.C. Hamill, J.H.B. Dean, and D.J. Jefferies, "Modeling of chaotic DC-DC converters by iterated nonlinear mappings," *IEEE Transactions on Power Electronics*, vol. 7, 1992, pp. 25-36.

[6] J.H.B. Deane, "Chaos in a current-mode controlled boost dc-dc converter," *IEEE Transactions on Circuits and Systems - I: Fundamental Theory and Applications*, vol. 39, 1992, pp. 680-683.

[7] I. Zafrany and S. Ben-Yaakov, "A chaos model of subharmonics oscillations in current mode PWM boost converters," *IEEE PESC Record*, 1995, pp. 1111-1117.

[8] I. Nagy, L. Matakas Jr. and E. Masada, "Application of the theory of chaos in PWM technique of induction motors," *International Power Electronics Conference in Yokohama Record*, 1995, pp.58-63.

[9] N. Hemati, "Strange attractors in brushless DC motors," *IEEE Transactions on Circuits and Systems - I: Fundamental Theory and Applications*, vol. 41, 1994, pp. 40-45.

[10] T.S. Parker and L.O. Chua, *Practical Numerical Algorithm for Chaotic Systems*. New York; Springer-Verlag, 1989.